Impact of sea−level rise and human activities in coastal regions: an overview

ZHAO Qing[1, 2, 3], PEPE Antonio[4], DEVLIN Adam[5, 6], ZHANG Shuangshang[7], FALABELLA Francesco[4, 8, 9], ZENI Giovanni[4], WANG Qiang[1, 2, 3], DING Jingzhao[1, 2, 3], DONG Danan[1, 2], LIU Min[1, 2, 3], XU Qing[7], LEI Xia[6], PAN Jiayi[5, 6]

1. *Key Laboratory of Geographic Information Science, Ministry of Education, East China Normal University, Shanghai* 200241*, China*;
2. *School of Geographic Sciences, East China Normal University, Shanghai* 200241*, China*;
3. *Chongming ECO Institute, East China Normal University, Shanghai* 200241*, China*;
4. *Institute for Electromagnetic Sensing of the Environment (IREA), Italian National Research Council,* 328 *Diocleziano, Napoli* 80124*, Italy*;
5. *School of Geography and Environment, Jiangxi Normal University, Nanchang* 330022*, Jiangxi, China*;
6. *Institute of Space and Earth Information Science, The Chinese University of Hong Kong, Shatin, Hong Kong, China*;
7. *College of Oceanography, Hohai University, Nanjing* 210098*, China*;
8. *University of Basilicata,* 85100 *Potenza, Italy*
9. *Institute of Methodologies for Environment Analysis (IMAA), National Research Council (CNR),* 85050 *Tito Scalo (PZ), Italy*

Abstract: Coastal regions are becoming increasingly vulnerable to flooding because of accelerating Sea-Level Rise (SLR), local ground subsidence, and changes in topography and morphology. Moreover, coastal areas are usually highly urbanized and increased human activities have an effect on the stability and preservation of the environment. For instance, the growing demand of new lands to accommodate the population and the industrial facilities in China has required the design and the deployment of land-reclamation projects from the ocean, with a marked impact on fragile coastal eco-systems. Specifically, the Yangtze River and Pearl River Estuary, two major estuaries of the world, have long been subject to intensive human activities over the past decades. Long-term ground subsidence evolution, topographic changes, and morphological variation of the coastal regions have drawn great attention. This paper provides an overview of well-established Earth Observation (EO) Remote Sensing (RS) technologies that are employed to continuously monitor the changes of urbanized regions. The combined use of EO-based DInSAR analyses along with the knowledge of the geomorphology of the coastal regions allows a more precise picture of the SLR risk in the investigated coastal regions. In this paper, we will concentrate on remote sensing technologies that allow the gathering of heterogeneous information, such as those based on the use of Synthetic Aperture Radar (SAR), satellite altimeters and tide gauge data. We will underline how human activities trigger changes in the living environment of coastal zones and the associated risks for the population. Observed coastline changes, coastal regions terrain subsidence, and offshore bathymetry have a pronounced effect on the increasing risk of flooding. Accordingly, we also present insights into some inundation model projections employed for evaluating the potential flooding risk in coastal regions.

Key words: flooding risk, sea-levelrise (SLR), ground subsidence, InSAR, anthropogenic geomorphologic changes

Citation format: Zhao Q,Pepe A,Devlin A,Zhang S S,Falabella F,Zeni G,Wang Q,Ding J Z,Dong D N,Liu M,Xu Q, Lei X and Pan J Y. 2020. Impact of sea−levelrise and human activities in coastal regions: an overview. Journal of Remote Sensing(Chinese). 24(S1): 202−218

1 INTRODUCTION

Global sea-level is rising, accompanied by increasing concerns about the growing urbanization of the world's low-lying deltaic coastal regions and related costal hazards inherent under scenarios of rising sea-levels (Nicholls and Cazenave, 2010; Woodruff et al., 2013). For instance, the projected SLR (Sea-Level Rise) of the Yangtze River Estuary could be up to 4 cm by 2030 (Cheng et al., 2018). Furthermore, the local relative SLR can be significantly affected by vertical ground motions, either due to natural processes

Received: 2019-10-21; **Accepted:** 2020-04-16

First author biography: ZHAO Qing (1982—), female, associate professor, her research interests are satellite remote sensing and its applications. E-mail: qzhao@geo.ecnu.edu.cn

Corresponding author biography: PAN Jiayi (1963—), male, professor, his research interests are coastal ocean dynamics, satellite oceanography, marine remote sensing physics, ocean numerical modelling, air-sea Interaction, ocean surface and internal waves. E-mail: panj@cuhk.edu.hk

(e.g., global isostatic adjustment (Stockamp et al., 2016), tectonics (Bentley et al., 2016; Higgins, 2016; Simms et al., 2016), sediment consolidation and compaction (Ingbritsen et al., 2000), upstream sediment load reduction (Yang et al., 2011)) or to human activities (e.g., groundwater extraction (Chen et al., 2016), land reclamation (Zhao et al., 2015; Xu et al., 2016; Pepe et al., 2016; Tian et al., 2016), sand mining (Zhang et al., 2010), deep waterway regulation (Cheng et al., 2018), and building constructions and consolidation (Wang et al., 2012; Chen et al., 2012)). The magnitude of deformation phenomena can be of the same order (or greater) than that due to climate-induced SLR. However, coastal ground motions are, in practice, often poorly known, and in many cases, little information is available about the patterns and time evolution of ground motion. It is therefore worthwhile to monitor coastal regions through advanced EO (Earth Observation) systems capable of detecting the ongoing surface deformation phenomena, recovering their spatial extent and following their temporal variability.

The changes in coastal topography and morphology can also influence other important factors that affect flooding hazards. Water level changes related to SLR can induce changes in the coastal response of astronomically-forced ocean tides (Devlin et al., 2017a; 2017b), typically via such mechanisms as changes in friction or changes in resonance of individual tidal components that may adjust the overall local behavior of tides at a regional scale, and thus, may change the inundation patterns of flood-prone regions. Both the YRE (Yangtze River Estuary) and PRE (Pearl River Estuary) have experienced variations in topography due to changes in natural forcing and intensive human activities, such as sediment deposition (Dai and Lu, 2014), erosion (Wei et al., 2015), sand excavation, dam construction (Yang et al., 2011; Dai et al., 2014) and land reclamation (Yang et al., 2011; Duan et al., 2016; Tian et al., 2016; Wu et al., 2016). In the past decades, human activities have also greatly impacted coastal environments by drastically modifying the coastal topography of the two estuary areas (Duan et al., 2016; Tian et al., 2016; Zhu et al., 2016). Furthermore, they have experienced dramatic changes in morphology (Zhang et al., 2015a; Wu et al., 2018; Wu et al., 2016; Zhu et al., 2016). Previous studies have shown that morphological changes of the PRE that have occurred in the past decades were mainly caused by human activities, such as land reclamation, sand excavation, and constructions of new infrastructure (e.g., the construction of the Hong Kong-Zhuhai-Macao Bridge) (Zhang et al., 2015b; Wu et al., 2018). Similarly, the YRE has also experienced long-term morphological variations (Mei et al., 2018; Wei et al., 2016; Zhu et al., 2016). The primary causes are intensified human intervention, including land reclamation, channel dredging (The Yangtze Estuarine Deeping Waterway project and the Qingcaosha Reservoir project) (Jiang et al., 2012; Pan and Ge, 2011), and upstream damming (over 50,000 dams constructed along the Yangtze River, including the massive Three Gorges Dam) (Yang et al., 2011, 2003). Human interference is predominantly controlling the morphological evolution of the Yangtze Estuary, and is expected to further complicate the morphology of the estuary (Luan et al., 2016).

To evaluate the combined risk of SLR, ground subsidence, and the changes in coastal topography and morphology of the investigated coastal regions, the availability of high-resolution DEM (Digital Elevation Models) of monitored coastal areas is mandatory. Added-value EO data-products, such as updated DEMs of coastal areas subject to SLR, and the time-series of terrain displacement and mean displacement velocity maps can be obtained by exploiting archives of SAR (Synthetic Aperture Radar) data with different spatial resolutions spanning a long time interval. The potential of the latest DInSAR methodologies (Massonet and Feigl, 1998, Ferretti and Prati, 2001, Hooper et al., 2001, Berardino et al., 2002, Mora et al., 2003) coupled to the capabilities of the newest SAR sensors (Covello et al., 2010; Torres et al. 2012) have enhanced spatial resolutions and revisit times of EO-based analyses, making it possible to investigate the displacement of Earth's surface with an accuracy of some millimeters in the LOS (Line-Of-Sight) direction, even in partially decorrelated areas. The improvements in using new SAR sensors are twofold. On one hand, the onboard placement of position tracking systems allows having detailed information on the satellite orbits, which is fundamental to retrieve the accurate phase displacement component relative to the investigated scenes. On the other hand, with advanced interferometric SAR techniques it is now possible to cover wide zones by processing huge loads of SAR data and to track the changes (i.e., displacement) of the scatterers that are present in the investigated areas, with a noticeable improvement in terms of precision and computation load.

The paper is organized as follows. Section 2 discusses the study areas and the problems that affect them. Section 3 discusses SLR and changing tides within the selected zones. In Section 4 and their subsections, we focus on the study of the Shanghai coastline changes, due to the natural events as well as to artificial intervention, with the help of advanced interferometric SAR techniques. We also give some insights on the role of interferometric SAR with regards to the study of human activities and their impact on the environment. Sections 5 and 6 address the offshore underwater topography and coastal flood modelling, respectively, both critical attention points to keep in consideration for future environmental evolutionary studies. Finally, Section 7 addresses possible ways to link the different proposed observation techniques and proposes a discussion and conclusion on the investigated scientific issues.

2 STUDY AREAS

The Yangtze River and Pearl River Estuaries are two of the largest eight river deltas of the world, covering an area of more than 5000 km^2. A rich supply of fine-grained suspended sediment is provided by the Yangtze River, which has contributed to the development of extensive tidal flats along the deltaic coast. The flats propagate outward, causing strong variations in erosion and deposition over a period of several years (Yang et al., 2003). The large amount of sediment supply and the high total discharge rate of the Yangtze River have also made it possible for the deltaic coast to reclaim land from the ocean. Hence, continuously reclaimed costal intertidal and wetland areas have allowed the development of new cities, ports, resorts, and industrial zones (Wang et al., 2014). In turn, rapid industrial development has caused widespread ground subsidence in the delta area, not only in the mega city of Shanghai, but also in many neighboring mid-sized cities, small cities, and towns.

The Yangtze River Estuary in China, is affected by SLR and by natural/anthropogenic deformation phenomena, making it clear the need of extended analyses for a better understanding of the mechanisms responsible for the observed surface modifications, and for the planning of actions devoted to risk prevention for populations living in coastal areas.

The Pearl River delta is the third largest in China, including the low-lying areas surrounding the Pearl River Estuary. Most of the delta plain is situated below local high-tide and storm surge levels (Wu et al., 2018). In recent decades, extensive land reclamation of muddy tidal flats has been increasingly carried out to combat fast urbanization and the expansion of agriculture, aquaculture, and industrial development (Wu et al., 2016). The delta region is exposed to natural disasters such as ground subsidence caused by soft soil compaction, Karst geomorphology, regional tectonics, and ty-

phoon-driven storm surges (Xu et al., 2016; Chen et al., 2012; Zhao et al., 2009; Wang et al., 2012; Wang et al., 2016; Chan et al., 2013).

3 SLR AND CHANGING TIDES

MSL (Mean sea-level) rise is a globally-observed phenomenon, with an average rise of +1.7 ± 0.2 mm yr^{-1} as calculated by historical tide gauges over 1900—2009 (Church and White, 2006; 2011), and +3.4±0.4 mm yr^{-1} for 1993-2016 as estimated from satellite altimetry (http://sealevel.colorado.edu/; Nerem et al., 2010). However, this rate is not spatially constant (Merrifield, 2009); for example, in the Western Pacific rates can be greater than +10 mm yr^{-1} (Merrifield, 2011). These rates are also not consistent over time and may accelerate in coming decades due to increased ocean warming (Domingues, et al., 2008), ice sheet loss, and anthropogenic activities (Slangen et al., 2016). The El Niño/Southern Oscillation (ENSO) is another contributing factor to sea surface anomalies in the Pacific (Kohl et al., 2007). Short-term MSL anomalies associated with ENSO are often much larger than long-term trends in MSL rates and major events (e.g., 1997—1998; 2015—2016) may yield widespread MSL fluctuations of 200 mm or more, especially in the Western Pacific.

MSL may influence or be correlated with tidal evolution in a variety of ways. Worldwide and regional studies of the Pacific (Jay, 2009), the North Atlantic (Ray, 2006, 2009; Ray and Foster, 2016) and China (Feng et al., 2015), among others, have revealed long-term changes in major ocean tide components. Such secular changes in tides may amplify the changes already brought by rising sea levels. In some locations, the tidal range may amplify during positive sea-level fluctuations, adding to the changes in total water levels, and increasing the probability of short-term flooding events such as nuisance flooding (a.k.a; "sunny-day flooding") where local flood levels can be exceeded even without storm activity (Moftakhari et al., 2015, 2017). In other locations, long-term changes to tidal range far outpace sea-level rise (e.g., Familkhalili and Talke, 2016), and help drive flood risk. Moreover, since storm surge is a long wave, factors affecting tides can also alter storm surge (Arns et al., 2017). Eventually, local water levels may breach existing flood defenses, as "tipping points" of coastal inundation are exceeded (Sweet and Park, 2014). If tidal evolution related to MSL variability exists at a location, then flood risk will not just be a superposition of present day tides and surge onto a higher baseline sea-level, as such predictions would be insufficient at locations with a high tidal sensitivity to water levels.

An additional form of MSL-related tidal variability has been observed, in that short-term fluctuations in MSL are often correlated to fluctuations in tidal amplitudes, denoted tidal anomaly correlations, or TACs. Amore useful metric is the combination of major tidal amplitudes as a proxy for the change in the full tidal range or highest astronomical tide, denoted δ-HATs. These forms of short-term water level variability have been documented in the Pacific Ocean (Devlin et al., 2017a, 2017b) as well as in the Atlantic (Devlin et al., 2019a), with results showing that significant TACs were observed in at least one tidal component at ~90% of all locations surveyed, with about half of all stations exhibiling a significant δ-HAT. Long-term trends can give a good indication of where baseline waters levels may advance but are less instructive in understanding the short-term patterns of flood events; the TACs and δ-HATs can give more insight into where tides have a higher sensitivity to water level fluctuations at multiple time scales and thus a better indication of the probability of tide-related nuisance flooding.

Historical tide records show that the sea level in coastal regions of China has increased 90 mm over the past 30 years (www.coi.gov.cn). The Yangtze River Delta and Pearl River Delta regions are vulnerable to SLR as low-lying coastal plains. Sea level rise faster in these regions largely due to the local subsidence (Ren, 1993). By using tide gauge measurements and satellite altimetry data to reconstruct the sea level change, He et al. (2014) found a relative sea level increase of 4.1 mm/yr in the Pearl River Delta from 1959 to 2011. In the Yangtze River Delta, the sea level rose at a rate of 2.6—3.0 mm/y from 1980 to 2011 with a significant spatial variation (Kuang et al., 2017).

Hong Kong and the PRD (Pearl River Delta) region contains many densely-populated urban metropolises with extensive coastal infrastructure, and substantial recent land reclamation projects. These coastal morphology changes along with sea-level rise may change the response of the local tides to the regional tidal variability and may contribute to total sea level TSL changes and nuisance flooding. Water levels in Hong Kong exhibit many variable features. The QB (Quarry Bay) tide gauge record in Victoria Harbor (1954-present) has an anomalous pattern of sea level rise. It has increased by +2.6 ± 0.5 mm yr^{-1} over the full record, but there are significant historical variations in this trend. From 1954 to 1987, the trend was negative, at −2 ± 0.5 mm yr^{-1}, yet from 1987 to 1999 it was strongly positive at +22.1 ± 2.3 mm yr^{-1}. From 1999 to 2007, MSL decreased at −13.1 ± 3.2 mm yr^{-1}, and since 2007, the rate has turned positive, at +7.4 ± 3.2 mm yr^{-1}. The Tai Po Kau (TPK) gauge in the semi-enclosed Tolo Harbor shows an overall MSL trend of +2.7 ± 0.5 mm yr^{-1} from 1963—2010, with similar temporally variable MSL rates. On a regional scale, satellite altimetry observations from 1993—2010 averaged over the South China Sea reveal an MSL trend of + 5.4 ±1.0 mm yr^{-1}, with some significant temporal and spatial variation from this trend (Li and Mok, 2012).

A recent regional study of Hong Kong showed that large TACs and δ-HATs are observed at a set of closely located tide gauges, though there can be considerable differences in tidal behavior even at closely located gauges, and certain locations are more sensitive to water-level-induced changes in tides, such as Victoria Harbor and Tai Po Kau (Devlin et al., 2019b). The TACs, δ-HATs, and some anomalous events in tidal amplitudes seen at the Quarry Bay and Tai Po Kau gauges show an amplified tidal response to MSL fluctuations in these harbor regions as opposed to more open-water locations, where individual TAC were sometimes significant, but not as much for the δ-HATs. The reason for the observed behavior may be due to changing friction or resonance induced by coastal engineering projects that are only significant at highly local (i.e., individual harbor) scales. Alternatively, the observed behavior could be related to regional SCS changes due to climate change (such as increased upper-ocean warming and/or regional stratification and internal tide generation) may also be a factor. It is difficult to separate the local engineering changes from regional climatic changes without closer investigations. However, even without exact knowledge of the relevant mechanisms, these anomalies do suggest that a pronounced change in tidal properties occurred around the year 2000 in Hong Kong, with the effect being most pronounced at gauges in semi-enclosed harbors. Overall, the tidal variability in Hong Kong may have significant impacts on the future of extreme sea level in the region, especially if the strong positive reinforcements hold or increase in coming decades. Short-term inundation events, such as nuisance flooding, may be amplified under scenarios of higher sea-levels that lead to corresponding changes in the tides, which may amplify small changes in water levels and/or reductions in friction due to harbor improvements. The δ-HATs and TACs illustrate that tidal variability can be positively reinforced at some locations, which may further agitate coastal flooding under MSL future rise. Since tides and storm surge are both

long-wave processes, the locations of strong tidal response may also experience an exaggerated storm surge in the near future. Similar issues are likely to be important in the Shanghai region, which is also very vulnerable to water-level related changes in the long-term as well as the short term. Unfortunately, there are not any recent hourly water level observational records from tide gauges publicly available along this part of the coast of China, so it is not yet possible to form as accurate of a picture of TAC-related variability in Shanghai as was possible in Hong Kong.

4 COASTAL AREAS CHANGES AND HUMAN ACTIVITIES

This section addresses the major changes of the investigated coastal regions, partially triggered by human intervention. We will show how the need for new lands have drastically changed the shape of the coastlines and have induced terrain subsidence of the new lands. Interferometric SAR techniques are used to detect the changes of the local topography and the ground subsidence signals.

4.1 STUDY OF THE COASTLINE CHANGES

The increasing demand of lands for industrial, residential, and public facility areas in highly populated coastal regions is fulfilled by the means of complex land reclamation engineering procedures. As a consequence, the coastline changes with time. Change detection of the actual coastline's orientation, position and shape (Lee, 1990) can provide basic information on the relationships between SLR, tidal currents and wave energy, land subsidence and human interventions. As pointed out in Wang et al. (2018), the contribution of SLR to coastal erosion is 3%~14% in the Yangtze River Delta, which has gradually increased under increased future sea-level rise. Thus, mapping coastline changes is fundamental to coastal management and land-use reasons, autonomous navigation, studying coastal erosion, planning of developing protection infrastructures, and assessing the increased risk of inundation at the coast (Ding and Li, 2011).

Coastline extraction is related to boundary detection and image segmentation in image processing and machine vision (Lee, 1990; Boak and Tunner, 2005). It has traditionally been performed by ground surveys, and more recently by using GPS data. For many decades, coastline modifications have been manually delineated by expert photo-interpreters by visual inspection of aerial photographs. However, these operations were costly and time-consuming. A step forward was represented by the advent of satellite (optical) remote sensing techniques, which have been demonstrated to have many advantages in monitoring surface-water boundaries and their extent (van der Werff, 2019; Pardo-Pascual et al., 2018). They provide repeat coverage at a relatively high spatial resolution and are usually less costly and time-consuming, especially for the survey of large geographic areas. However, despite these advantages, optical satellite remote sensing also has some limitations. When using optical data, coastline detection is strongly affected by cloud coverage, solar illumination, and meteorological conditions. At variance with optical data, microwave remote sensing data are not affected by clouds but the presence of the speckle effect (Lee, 1990), which is generated by the coherent signal-scattering within SAR resolution elements and complicates the detection problem. It has been shown in (Lee, 1981) that the speckle distribution is quite accurately described by a multiplicative noise model and different approaches that require an initial speckle reduction step have been presented in the literature (Lee, 1990, Fugura et al., 2011). The majority of these methods rely on the detection of coastline changes by inspecting the maps of the backscattered sigma naught signals, obtained after the calibration of the amplitude SAR images (Freeman, 1992). Other approaches use the information on the coherence between couples of complex-valued SAR images, that has been proven to be a significant discriminant between land and sea (Dellepiane, 2004). Very recently, an innovative approach, which is able to work with more than one image at full spatial resolution has been proposed in (Baselice and Ferraioli, 2013). The method is developed in Bayesian stochastic estimation and MRF (Markov Random Field) frameworks, and is based on the estimation of the spatial correlation among neighboring pixels.

Coastline detection is closely linked to the investigation of the subsidence deformation of the coastal regions, and in particular of the ocean-reclaimed platforms. In particular, some investigations have already been carried out over Nanhui New city, Shanghai, China for the extraction of the coastline (Ding and Li, 2014) and for studying the deformation of the ocean-reclaimed lands (Pepe et al., 2016). Nanhui has been historically experiencing variations in landscape due to changes in natural forcing and intensive human activities, such as sediment deposition, erosion, sand excavation, dam construction, and land reclamation (Yang et al., 2011). Fig. 1 shows the extracted shorelines of Nanhui New City of Shanghai obtained from Sentinel-1A SAR images

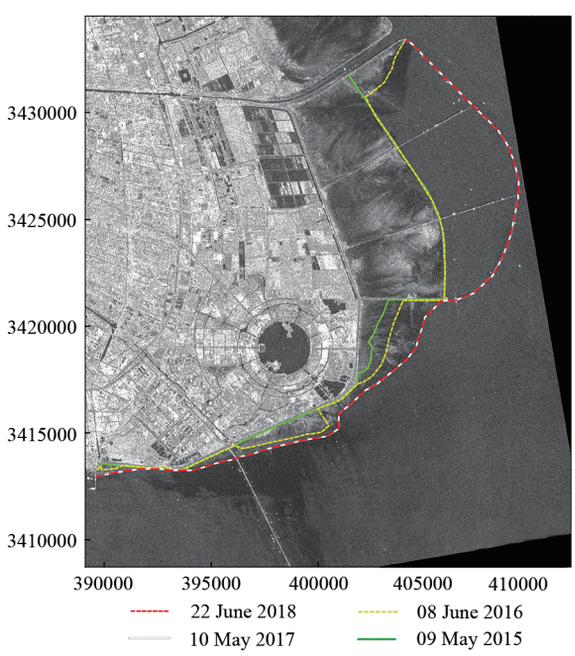

Fig.1 Mapping of the extracted shorelines of Nanhui New City of Shanghai from 2015 to 2018 as obtained from Sentinel-1A SAR images.

4.2 ANTHROPOGENIC GEOMORPHOLOGIC CHANGES

There are a number of global DEM (Digital Elevation Models) freely available to the public. The SRTM (Shuttle Radar Topography Mission) DEM was deployed in 2000 by spaceborne SAR (Synthetic Aperture Radar). Although SRTM DEM is of relatively stable accuracy and is commonly used (Jarvis et al., 2008; Yang et al., 2011), it is relatively old for updated inundation mapping, especially for the estuary areas with time-varying topography. Comparatively, The ASTER (Advanced Spaceborne Thermal Emission and Reflection Radiometer) Global Digital Elevation Model (GDEM) is another open DEM data source. Version 2 of ASTER GDEM

contains new datasets from 2000 to 2010, making it relatively new. However, the accuracy of ASTER GDEM has attracted controversy due to the anomalies and noises caused by optical imaging limitations (Tachikawa et al., 2011a, b; Mukherjee et al., 2013). The other open source DEMs are the Global 30-Arc-Second Elevation Data Set (GTOPO30) and the Global Multi-resolution Terrain Elevation Data 2010 (GMTED2010). GTOPO30 was developed by U. S. Geological Survey (USGS) in 1996 at a horizontal resolution of 1km for the entire global land surface (Gesch, 1999). GMTED2010 is an enhanced global elevation model developed by USGS and the NGA (National Geospatial-Intelligence Agency) to replace GTOPO30 (Danielson and Gesch, 2010). Comparing with GTOPO30, GMTED2010 provides a new level of level of detail in global elevation data. These products are suitable for continental and global-scale applications.

Table 1 Open access DEM data sources

	ASTER GDEM	SRTM DEM	GTOPO30	GMTED2010
Instruments	The Advanced Spaceborne Thermal Emission and Reflection Radiometer (ASTER) onboard NASA's Terra spacecraft	C-band and X-band Synthetic Aperture Radars onboard NASA's space shuttle Endeavour	Fusion of eight data sources	Fusion of 11 raster-based elevation sources. The primary source dataset is SRTM DEM of NGA.
Data collection time	2000—2008 (Version 1) 2000—2010 (Version 2)	2000	1996	2010
Resolution	30 m 20 m	30 m (in the US) 90 m (in the rest of the world)	1 km	250 m 500 m 1 km
Vertical Accuracy	20 m (Version 1) 13 m with controversy (Version 2)	16 m	30 m	28 m 31 m 34 m
Coverage	83 degrees north—83 degrees south	60 degrees north—56 degrees south	the entire global land surface	Global coverage of all land areas
Advantages	It provides the global current elevation data with relatively higher resolution	It covers most of global land surface with relatively higher resolution	It covers the entire global land surface	It provides the global current elevation data.
Disadvantages	ASTER GDEM is severely affected with random noise and anomalies	The previously released SRTM DEM-3 v4.1 is limited by 90 m resolution and inaccurate void-filling	coarse resolution to satisfy the demands of costal inundation mapping and assessment	coarse resolution to satisfy the demands of costal inundation mapping and assessment

Accurate and up-to-date elevation data of the time-varying topography of the dynamic coastal area is crucial for assessing and mapping potential inundation areas. The open access DEM data sources are of limited spatial and temporal resolution. Use of this dataset makes it difficult to satisfy local-scale flood risk assessment and mapping studies. To better address the terrain dynamics, the new generation of the spaceborne SAR (Synthetic Aperture Radar) mission, TanDEM-X, has recently been specifically deployed for the generation of updated profiles with high resolution of the terrain (Krieger et al., 2007). The TanDEM-X mission has the innovative capability of collecting bistatic data with short along-track baselines, and generating seamless global DEM with high resolution.

We calculated the TanDEM-X DEM of Nanhui New City of Shanghai with bistatic interferometry. The elevations of TanDEM-X DEM, which are referenced to the WGS84 (G1150) ellipsoid, are then converted to orthometric heights referenced to the EGM 96 Geoid as consistent with the reference datum of SRTM/ASTER elevations for comparison purposes. The DEMs of Nanhui New City are shown in Fig. 2. A grid spacing of 6 m is selected for the TanDEM-X DEM product. The relative theoretical vertical accuracy of the TanDEM-X DEM is 2 to 4 m depending on the slope (Krieger et al., 2007). The theoretical accuracy and actual DEM performance of bistatic TanDEM-X InSAR were verified by Weigt et. al., (2012). Their verification shows that when slopes are smaller than 20%, and height of ambiguity is about 20 m, the relative vertical error is around 1.5 m.

4.3 INTERFEROMETRIC SAR ANALYSES FOR THE MONITORING OF GROUND SUBSIDENCE

InSAR (Synthetic Aperture Radar Interferometry) (Massonet and Feigl, 1998) is a consolidated technique used to measure crustal deformation, which can be associated with volcanic and seismic activity, other natural phenomena (e.g, flooding, landslides, etc) or human-induced mechanisms (e.g., the deformation of buildings in urban areas, the consolidation of new lands in ocean-reclaimed regions, etc). InSAR exploits the phase difference of a pair of SAR images collected at two different times from slightly different orbital positions. The complex-valued SAR signals can be expressed as follows (Franceschetti and Lanari, 1999)

$$\begin{aligned} i_1 &= \gamma_1 \exp\left(-j\frac{4\pi}{\lambda}r_1\right) \\ i_2 &= \gamma_2 \exp\left(-j\frac{4\pi}{\lambda}r_2\right) \end{aligned} \tag{1}$$

where γ_1 and γ_2 are the reflectivity functions and r_1 and r_2 are the sensor-to-target range distances at the two acquisition times. By

considering the imaging geometry shown in Fig. 3, the expression of the phase difference between the two SAR images (Franceschetti and Lanari, 1999) is given as follows

$$\Delta\varphi = \frac{4\pi}{\lambda}\frac{b_{\perp}}{r\sin\vartheta}z + \frac{4\pi}{\lambda}d_{\mathrm{LOS}} + \Delta\varphi_{\mathrm{atm}} + \Delta\varphi_{\mathrm{orb}} + n \quad (2)$$

where the height topography is given by z, the radar line-of-sight projection of the deformation is given by d_{LOS}, λ is the operational wavelength,ϑ is the side-looking angle, $b_{\perp}$ is the InSAR couple perpendicular baseline, $\Delta\varphi_{\mathrm{atm}}$ is the phase term that accounts for inhomogeneities of the atmosphere between the two passes of the sensors over the same area, $\Delta\varphi_{\mathrm{orb}}$ is the phase term due to the inaccurate knowledge of the orbital values related to the interferometric pair, and n accounts for the phase noise signal. The InSAR technique has first been applied to measure the height z of the ground. Further, InSAR has evolved to monitor the deformation of the ground (dLOS) with the advent of the Differential SAR interferometry (DInSAR) technique. The limits and potential of DinSAR technique have been addressed in several papers (see, for instance, the review paper in (Pepe and Calo, 2017)).

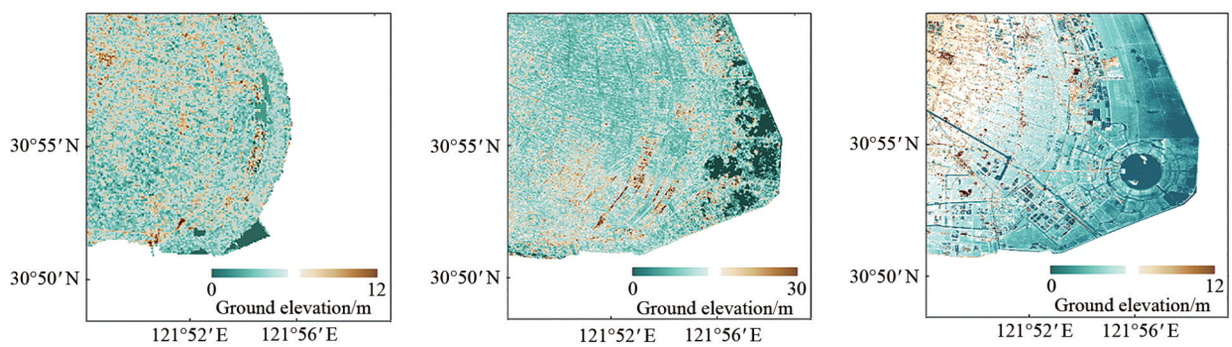

(a) SRTM DEM (b) ASTER GDEM (c) TanDem-X Dem

Fig.2 DEMs of Nanhui New City. SRTM DEM ASTER GDEM and TanDEM-X DEM obtained with bistatic interferometry

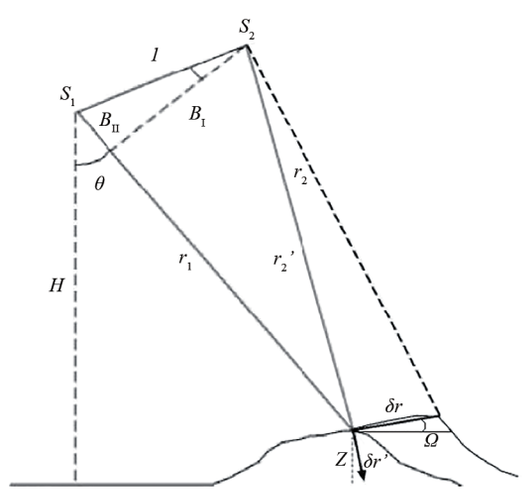

Fig.3 InSAR Geometry.

Historically, InSAR has been applied for investigating single deformation episodes. However, over the last 20 years, interest has grown for generating displacement time-series through the analysis of sequences of long-lasting SAR data. To this aim, advanced multi-pass InSAR methods (Ferretti and Prati, 2001, Hooper et al., 2001, Berardino et al., 2002, Mora et al., 2003) have been developed. Two main categories of advanced DInSAR techniques have been proposed. They are often referred to as PS (Persistent Scatterer) (Ferretti and Prati, 2001, Hooper et. al., 2001) and SB (Small Baseline) (Berardino et al., 2002, Mora et al., 2003) techniques. The class of SB methods includes the algorithm known to as Small Baseline Subset (Berardino et al., 2002). It was developed in 2002 and it is based on the processing of sequences of SB interferograms. Accordingly, selected SAR data can be arranged in several disjointed (time-overlapped) subsets that are separated by large baselines. These subsets are independent of each other, and this gives rise to an underdetermined problem for the time-series inversion, which can be solved by searching for a minimum norm least squares solution via the SVD (Singular Value Decomposition) method (Strang et al. 1988). A method that permits to recover the InSAR deformation time-series of distributed targets on the ground is also SqueeSAR (Ferretti et al., 2011), which operates on interferograms computed at the same spacing of the full resolution ones but following an ad-hoc low-pass filtering step.

4.3.1 INSAR EXPERIMENTAL RESULTS

In this subsection, some experimental InSAR results achieved over the YRE and PRE regions are presented. The area is affected by deformations due to the soil consolidation of the ocean-reclaimed platforms, as evidenced in (Pepe et al., 2016). Previous studies, based on processing a set of first- and second-generation SAR data collected from the ASAR instrument onboard the ENVISAT mission and the COSMO-SkyMed (CSK) SAR sensors constellation of the Italian Space Agency, respectively, have revealed that the deformation is expected to continue over time with decreasing rates, as foreseen by a proper geotechnical model (Zhao et al., 2015, Pepe et al., 2016). The SBAS algorithm (Berardino et al., 2002) has been applied to generate the ground deformation maps. In particular, the EMCF (Extended Minimum Cost Flow) algorithm (Pepe and Lanari, 2006) has been used to unwrap the selected network of DInSAR interferograms. Note that the EMCF technique is based on the well-known network-programming paradigm (Costantini, 1998), which is extended to work both on the temporal and spatial grids. Fig. 4 shows the mean ground deformation velocity maps of the Shanghai megacity coastal zone revealed by processing a sequence of 69 CSK SAR data acquired between December 7, 2013 and February 28, 2018 (see Fig. 4a) and by processing a set of 31 ASAR images collected from February 26, 2007 to May 31, 2010 (Fig. 4b). Fig. 5 shows a zoom of the ground deformation map, as revealed using the CSK dataset, in correspondence with Dishui Lake. Fig. 5 shows the ground displacement time-series related to three investigated points (A, B and C) that are located around the lake. The analysis has been performed by properly adapting the original SBAS codes (Berardino et al, 2012; Lanari et al., 2004) for the analysis, at full spatial resolution scale, of medium-to-low coherence areas, as originally addressed in (Falabella et al., 2018). The results of this analysis show that the most unstable

zones are those where the ocean-reclamation processes started earlier (Zhao et al., 2019).

A second experiment was carried out over the PRE region to study the recent deformation signals affecting the investigated area. Using three sets of ASAR images spanning the time period from 2007 to 2010, Wang et al. (2012) previously studied the surface deformations affecting the city of Shenzhen, and estimated the impact of the urban development and the SLR of the PRD region. In this study, we show the results of a preliminary investigation of the deformation of the entire PRD region by initially focusing on the period from October 2016 to March 2017, to show the capability of mapping and the enhanced spatial coverage of the European Copernicus Sentinel-1 (Torres et al., 2012) SAR image database.

The two experiments shown here demonstrate how in two of most important coastal regions of China, intensive urban sprawl (Deng et al., 2008; Chen et al., 2012), triggered by economical and societal reasons, has been drastically changing the environment. The risk for population not only derives from the increased air (Chan and Yao, 2008) and water pollution (Gong et al., 2012), but there is also a direct relationship between global climate change and coastal instability. New lands are subjected to natural self-compaction mechanisms and tend to subside, requiring dozens of years to reach a condition of stability. At the same time, current SLR and the unceasing change of coastlines considerably increase the risk of flooding in the new lands. Radar technology can help in the continuous monitoring of the evolution of surface changes, and the obtainable results are beneficial for urban planners and local authorities. Additionally, radar data can provide valuable information for planning suitable measures for enhancing the resilience to natural disasters by identifying and restoring the areas that are more prone to be inundated. Knowledge of the present-state of ground deformation rate, SLR and terrain height as well as the foreseeing of their changes over time is essential.

5 OFFSHORE UNDERWATER TOPOGRAPHY

A bathymetric measurement of shallow water is of fundamental importance to coastal environment research and resource management. A traditional bathymetric survey uses a shipboard sonar, single-beam, or multi-beam sounding system, which can provide high-precision data but is costly and inefficient. With the development of remote sensing techniques, the shallow water depth can be measured with high efficiency. A spaceborne SAR, in particular, provides valuable information of shallow water topography in all-weather and day-night conditions with a high spatial resolution (a few to tens of meters). In 1969, De Loor et al. discovered that under suitable conditions (moderate wind and strong tidal current) sea bottom topography may be visible in real aperture radar images (De Loor et al., 1978; De Loor, 1981). Alpers and Hennings (1984) proposed the first full model for the imaging mechanism of shallow water topography as a three-step process:

(1) The interaction between tidal currents and bottom topography, which results in modulations in the surface flow velocity;

(2) The interaction between the variable surface flow and the short surface water waves;

(3) The interaction between the short surface water waves and radar signals.

Many bathymetry models using SAR data based on this theory have been developed, including an operational system called the BAS (Bathymetric Assessment System), which can detect accurate shallow water depths from SAR imagery by combining limited samples of in situ observations with an iterative procedure. A number of applications show that the efficiency of bathymetric surveys can be increased considerably by applying the BAS, which also has been used operationally as a commercial service by the company ARGOSS in the Netherlands to support bathymetric surveys (Calkoen et al., 2001). Using SAR images, Jin et al. (1998) obtained a solution to the shallow water depths in the two-dimensional shallow water dynamic equations using a first-order analytical expression of the SAR image gray level. A function proportional to the radar backscatter cross section σ_0 is defined to simulate the radar image gray tone level and the inversion method is the minimum deviation solution. Huang and Fu (2004) developed a straightforward numerical model for shallow water bathymetry retrieval from SAR imagery and its calculation procedure based on the SAR imaging mechanism of sea floor topography. Using shallow water bathymetry, the SAR imaging mechanism, and the M4S (Model for Fully Two-dimensional Simulation), a microwave scattering imaging model for oceanic surface features, Fan et al. (2011) developed a method for shallow water depth retrieval from spaceborne SAR images. Their results show that SAR images are useful for shallow water depth retrieval and suggesting that this method is convergent and applicable. More recently, (Renga et al. 2014; Stewart et al., 2016) developed a bathymetry retrieval algorithm able to perform the direct inversion limiting the need for a priori information or in situ measurements, and for human intervention in the processing chain. Their results show that dense coverage and metric accuracy can be achieved even when the current is not strong enough to dominate the SAR response. Based on the shoaling and refraction of long surface gravity waves as they propagate shoreward, Bian et al. (2017) developed a method to detect underwater topography in coastal areas using high-resolution fully polarimetric SAR data, which can provide detailed information on scattering mechanisms that could enable the target or structure to be identified. Their results indicate that a scattering mechanisms-based methodology is more effective than only using the single polarization SAR data for underwater topography detection; this will inspire further research on underwater topography detection with fully polarimetric SAR data.

Other models for SAR bathymetry have been developed which are based on different theoretical mechanisms, such as changes in wave height and wave energy dissipation resulting from waves breaking over varying topography in the surf zone (Wackerman et al., 1998), and the refraction and shoaling of long swell waves due to underwater bottom topography in shallow areas (Brusch et al., 2011, Mishra et al., 2014, Boccia et al., 2015, Bian et al., 2018).

For tidal flats, the areas inundated during high tide and exposed

The obtained results show that the coastal area, which has been subjected to severe reclamation procedures over the years, is now relatively stable, with average deformation rates, at most, of a few millimeters per year, except for some isolated "hotspot" areas, which are highlighted in Fig. 5, where the measured deformation rate exceed 5 cm/year. The selected "hotspot" areas belong to coastal zones and the observed deformations are clearly due to human activities, as the entire identified zone is located over new lands reclaimed from the ocean. Further extended investigations will be carried out to characterize the state of the deformations of this region using Sentinel-1 data, and this will be the subject of future studies.

during low tide, waterline method with remote sensing data is currently considered to be the most useful approach to generate the topographic maps of the intertidal zone (Ryu et al., 2008, Mason et al., 2010, Kang et al., 2017, zhang et al., 2018). The waterline method makes use of the ever-shifting boundary between tidal flats and adjacent water areas, whose position can be regarded as a quasi-contour line of the topography. Using three Sentinel-1A SAR images acquired at different tidal levels, i.e., low, middle and high tidal levels, as shown in Fig.7, we generated the topographic map of the Subei Bank tidal flats by the waterline method. The results show that in general there is a good agreement between the derived elevation and in-situ topographic data, implying that the waterline method based on SAR images can be used for large scale tidal flats.

The conventional bathymetry detection method using optical

Here, we present a case study to detect shallow water depth using satellite optical imagers. The study area is the Port Shelter in the Hong Kong coastal water with previous in-situ water depth observation data. The case study uses the high spatial resolution data of the RapidEye satellite system. RapidEye system consists of 5 earth observation satellites owned and operated by Planet Labs, providing 5-meter resolution imagery (https://earth.esa.int/web/eoportal/satellite-missions/r/rapideye). The images used in this study were acquired on November 16, 2014 in clear sky, and a water depth retrieval algorithm based on semi-analytical radiation transfer model is employed to perform water depth retrieval with the high-resolution satellite data in selected experimental areas (A, B, C, D in Fig. 8).

We employ the Fourier transform to filter the high-frequency noise for the blue (440—510 nm) and green bands (520—590 nm). The atmospheric correction is applied to the satellite imagers with first-principles atmospheric 'correction' algorithm (FLAASH, Adler-Golden et al., 1999). After the satellite image pre-processing, the blue and green bands of the RapidEye satellite data are used as the input data for the water depth retrieval model. Then the accuracy evaluation of the water depth retrieval results is conducted Fig. 9 shows comparisons between satellite data-retrieved water depths and measured water depths at locations in arees A(a,b), B(c, d) C(e,f) and D(g,h). The left pane of Fig.9(a)(c)(e)(g) shows comparison results based on the blue band algorithm and the right panel (b, d, f, h) reveals those based on the green band algorithm. Table 2 lists absolute error and relative error of the water depth retrieval results. The relative error is below 20%; the absolute error varies with the depth, and is ≈0.5 m for the water depth of ≈7 m. The case study suggests that high spatial resolution of depth in shallow water can be obtained based on satellite optical imagery with good accuracies.

6 COASTAL FLOOD MODELLING

Estuaries, the transition zone between rivers and the open sea, are the most vulnerable areas to river and marine floods. Rising sea level, subsiding costal lands, and changing coastal topography and morphology may also increase flooding risks induced by storm surges with augmented frequency and severity. In order to simulate inundation under different scenarios, numerical models have been developed. The inundation model called LISFLOOD-FP, which is a simple 2D raster-based model, has previously been applied to predict maximum flood inundation extents at a number of coastal sites (Bates and De Roo, 2000; Bates et al., 2005). Two-dimensional hy-

satellite imagery has been proven to be a useful technology. A simple water reflection model of the ratio algorithm was used to retrieve the nearshore bathymetry with optical imagery (Polcyn et al., 1970). Lyzenga (1978) developed a general algorithm for shallow bathymetry detection with better discrimination of bottom materials. With the diffuse attenuation coefficients explicitly expressed as functions of in-water absorption and backscattering, a semianalytical model for retrieval of shallow water bathymetry was developed, which can be used to process hyperspectral remote sensing data (Lee et al., 1998). Recently, Geyman and Maloof (2019) applied the CBR (Cluster-Based Regression) algorithm to analyze multispectral Satellite Imagery in a portion of the Great Bahama Bank and achieved a mean absolute error of 0.19 m for the bathymetry detection.

drodynamic models (MIKE 21 and FloodMap-Inertial) have been employed to simulate flood magnitudes under different scenarios and model fluvial flood risks in the coastal areas of Shanghai (Wang et al., 2018; Yu, 2010; Yu and Lane, 2006a, 2006b, 2011; Yin et al., 2015). The flood vulnerabilities in the cities of Pearl River Estuary have also been evaluated. These results show that the exposure and sensitivity of coastal mega cities including Hong Kong, Macao, Shenzhen, and Guangzhou are very high (Huang et al., 2018; Pan et al., 2017; Yang et al., 2014). Yin et al. (2019) integrated 2-D numerical flood model and multi-temporal InSAR techniques to investigate flood hazard of Lingang New City in Shanghai in the background of sea-level rise, changes of coastal topography, and long-term ground subsidence.

7 DISCUSSION AND CONCLUSIONS

The coastal flood vulnerabilities of Yangtze River Estuary and Pearl River Estuary are currently being amplified by the combined effects of accelerating SLR, long-term and short-term tidal evdution time-dependent ground subsidence, changes of coastal topography and morphology as well as natural hazards. The examples of estuary regions affected by the combination of SLR, significant modifications over time, and natural hazards provided here make clear the need of extended analyses of understanding the mechanisms at the base of the coastal surface modifications, estimating the future regional sea level changes and evaluating the potential submerged land areas. The use of well-established remote sensing technologies, based on the joint exploitation of data collected at different spectral wavelengths, the advanced DInSAR techniques, satellite altimeter and tide gauge data as well as the inundation model projections can be employed for these purposes. The scientific results shown in this review paper represent an asset for the planning of present and future activities devoted to the monitoring of such fragile environments. These analyses are essential to assess the factors that will continue to amplify the vulnerability of the low-elevation coastal zones and increase the exposure to natural risk for the population living in the coastal regions.

Identifying and using global and non-invasive remote sensing (active and passive) methodologies allows discriminating the zones within the selected coastal areas that have historically been affected by intensive human activities (such as land reclamation) and natural disasters (such as typhoon and storm surges), and identifying those which can be more prone to significant changes and disasters in the near future. This is usually done by analyzing the effects that these phenomena have produced on the territory. Optical satellite images can continuously and frequently monitor the evolution of shoreline on the timescale of decades or even longer. SAR imagery can not only detect shoreline during all-day and all-weather, but al-

so derive topography changes of coastal areas and shallow water topography. Assessing, developing and handling efficient disaster management cycles using EO (Earth Observation) products, in the cooperation with the factors in charge of the security of the territory, the scientists and the citizens is beneficial for the construction of a society that is more resilient to disasters, also partly triggered by human activities, such as the uncontrollable cities sprawling, coastal erosion and the global climate changes.

Finally, we would like to remark that concerning these scientific concerns, the ESA-MOST Dragon initiative (http://dragon4.esa.int/files/DRAGON_2018_broch_STATIC. pdf [2019-10-21]) has represented an opportunity to develop a community of EO experts in Europe and China with the aim to investigate how remote sensing methodologies can routinely recover valuable information on the state of Earth environment and its modifications over time.

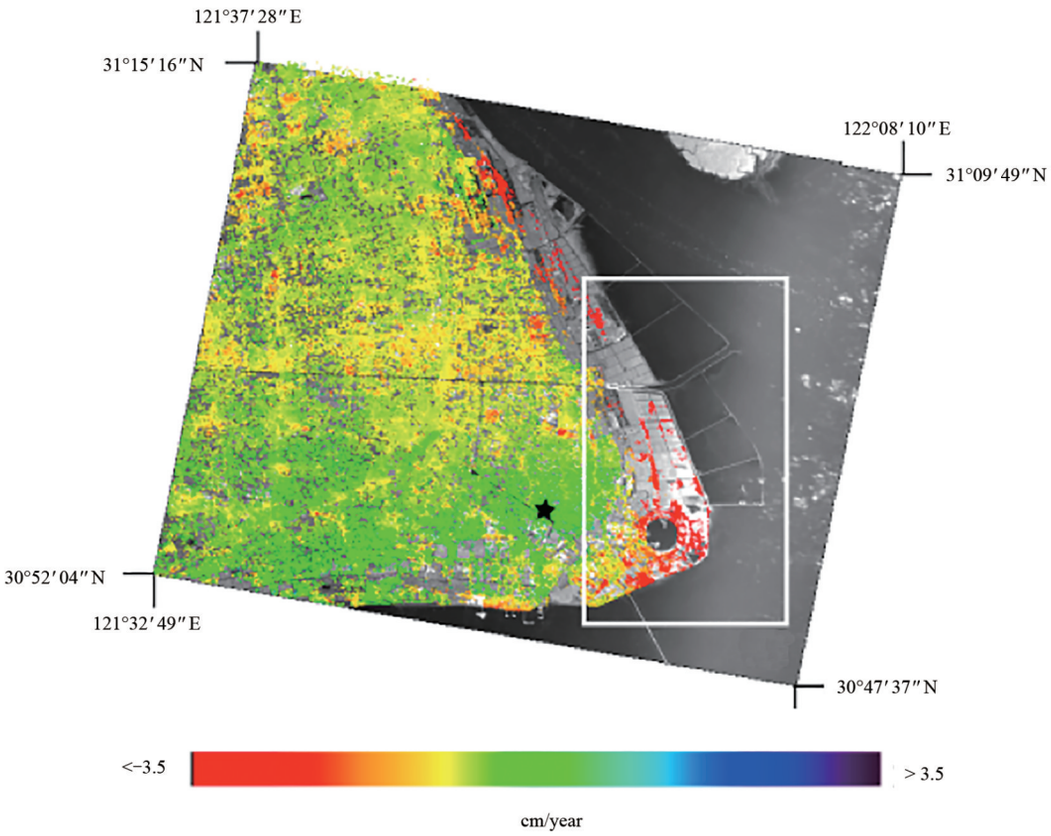

(a) CSK SAR data

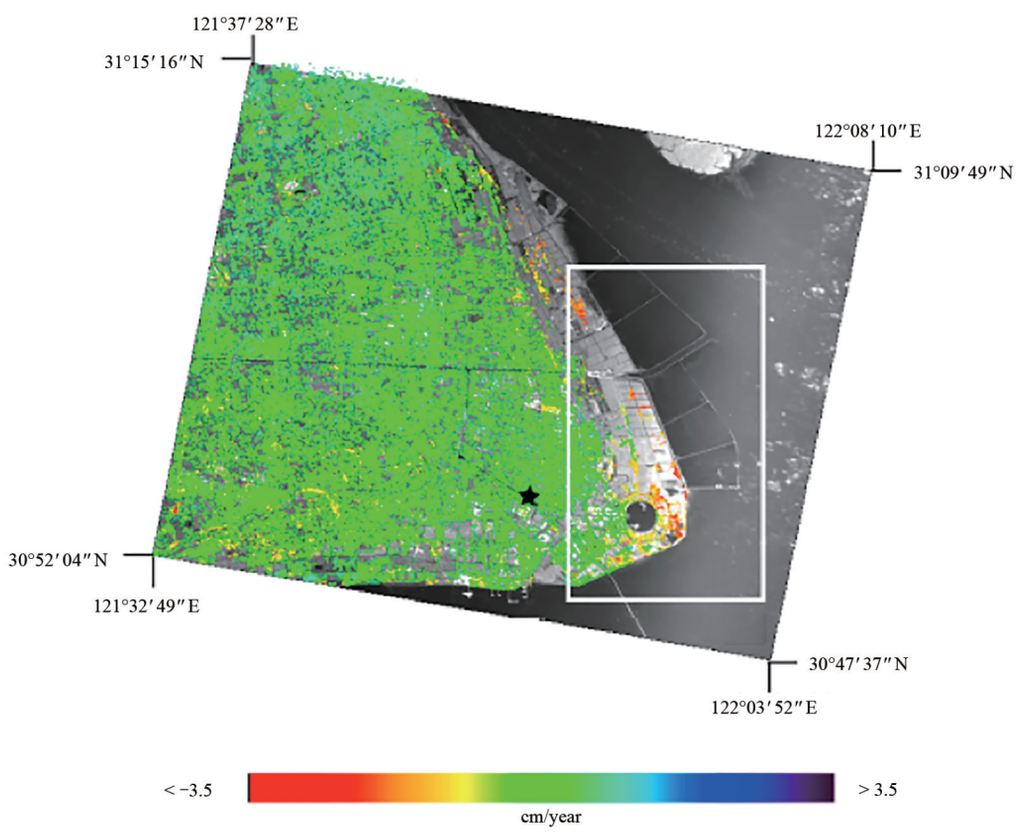

(b) ASAR SAR data

Fig.4 Ground displacement map of the coastal area of Shanghai obtained using CSK and ASAR SAR data. The maps are overimposed to a geolocalized CSK SAR amplitude image of the investigated area.

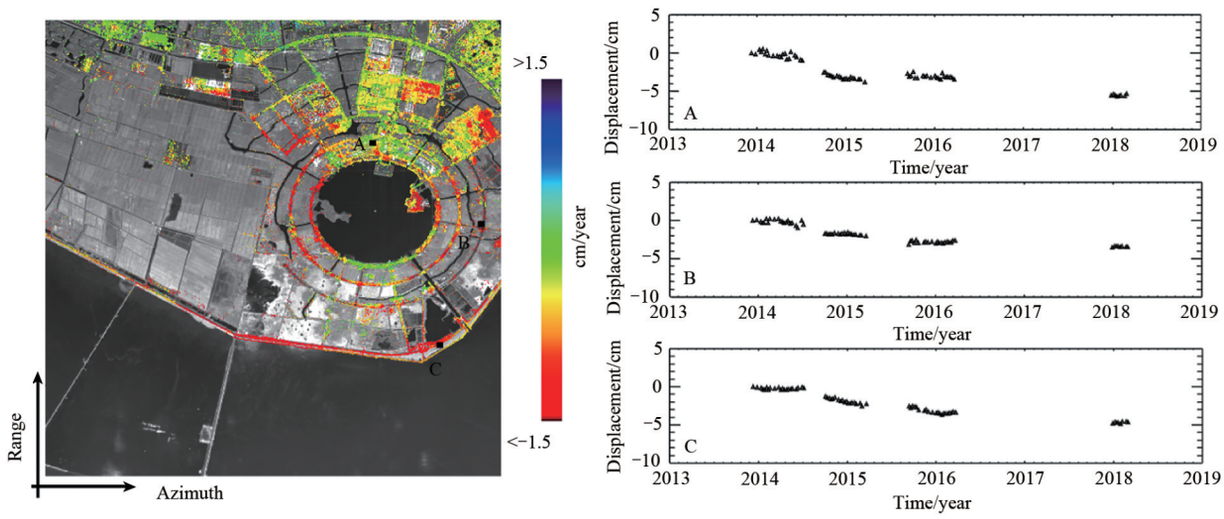

Fig.5 Map of the mean displacement rate of the Lingang New City from 2014 to 2018, as revealed by the CSK SAR constellation. Plots of deformation time-series of three selected points, labelled to as A, B, C are also shown.

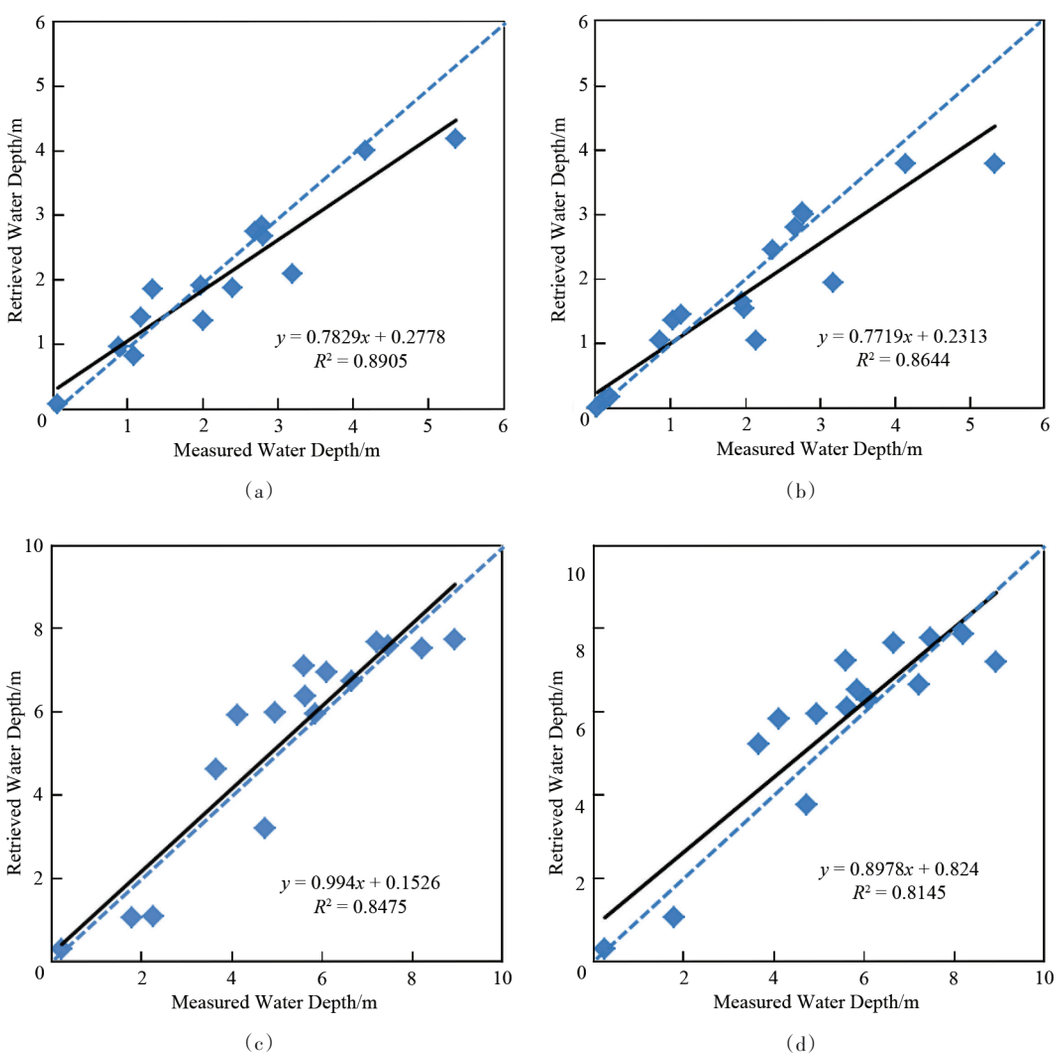

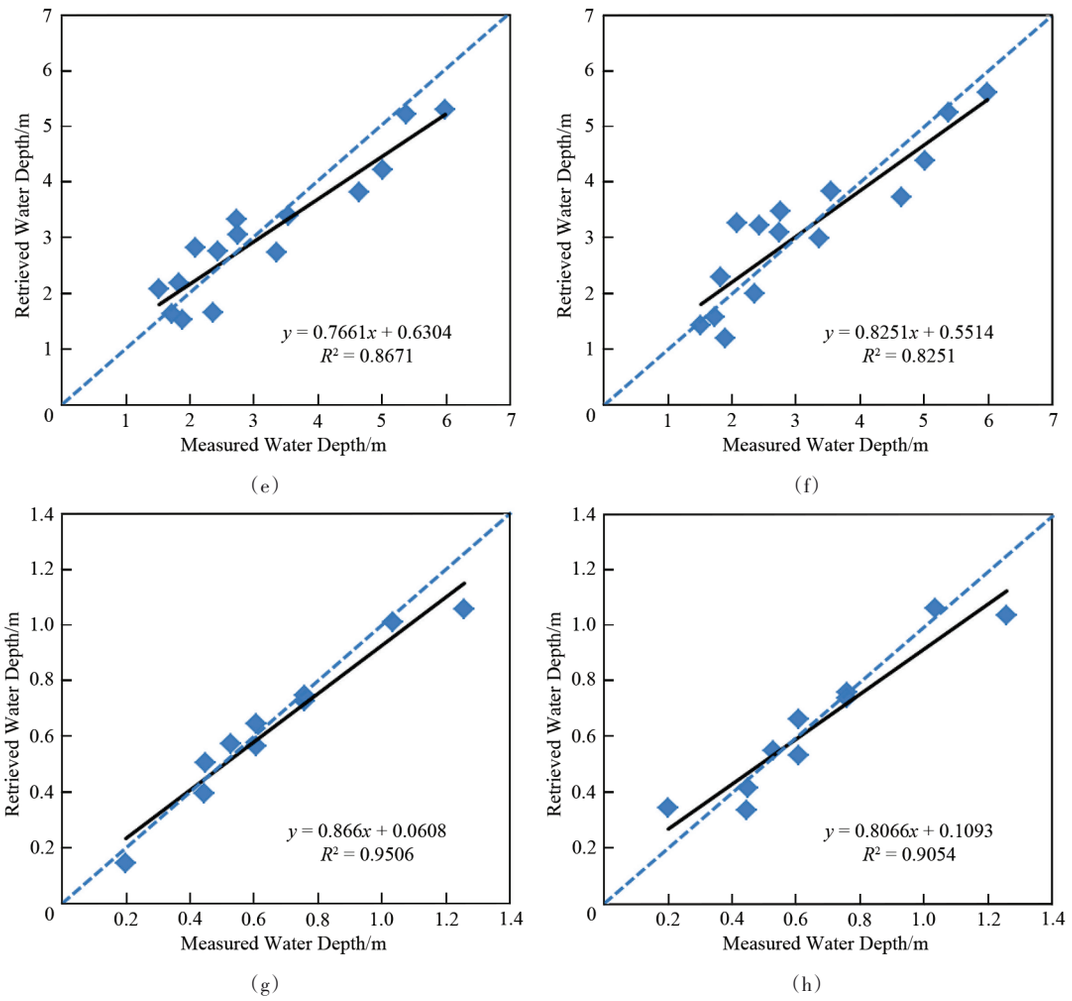

Fig.9 Satellite image-retrieved water depth versus in-situ observation data. The dash lines represent 1∶1 lines.

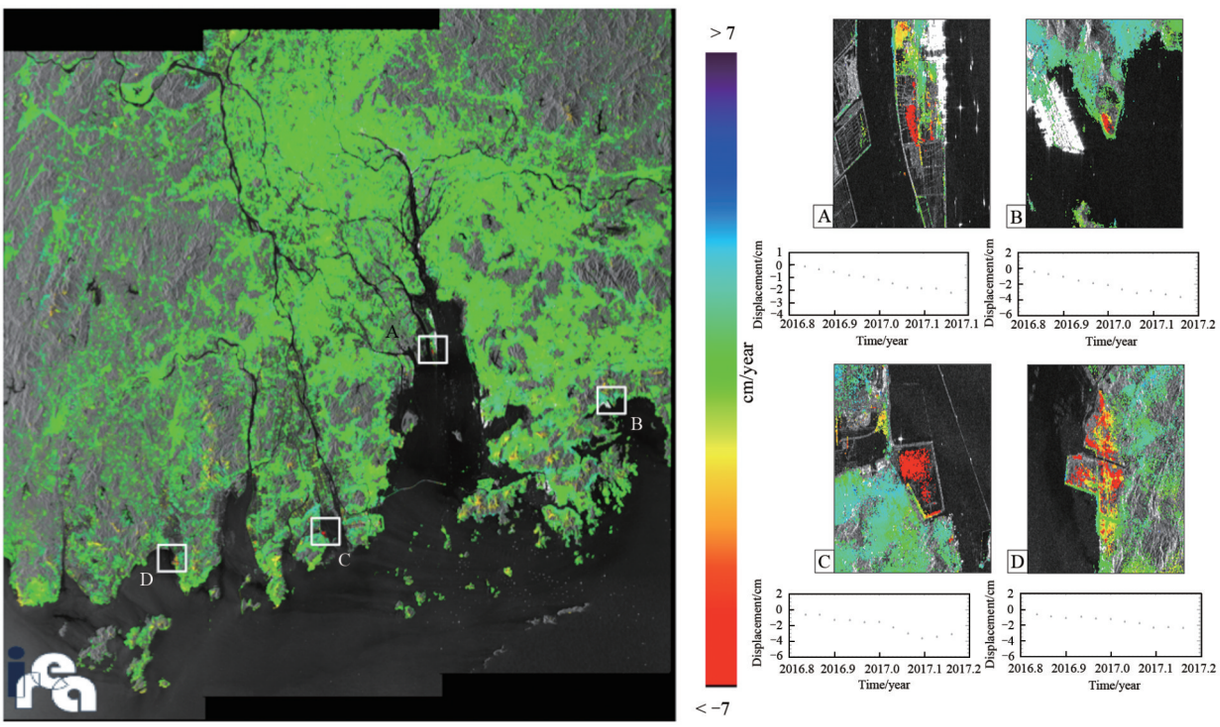

Fig.6 Map of mean displacement rate of the PRE region from September 2016 to March 2017, as revealed by processing a set of Sentinel-1 SAR data. Four regions, labeled to as A, B, C, D, characterized by significant deformations rates are highlighted. Plots of the surface deformation time-series in correspondence to four selected pixels in the highlighted zones are also shown.

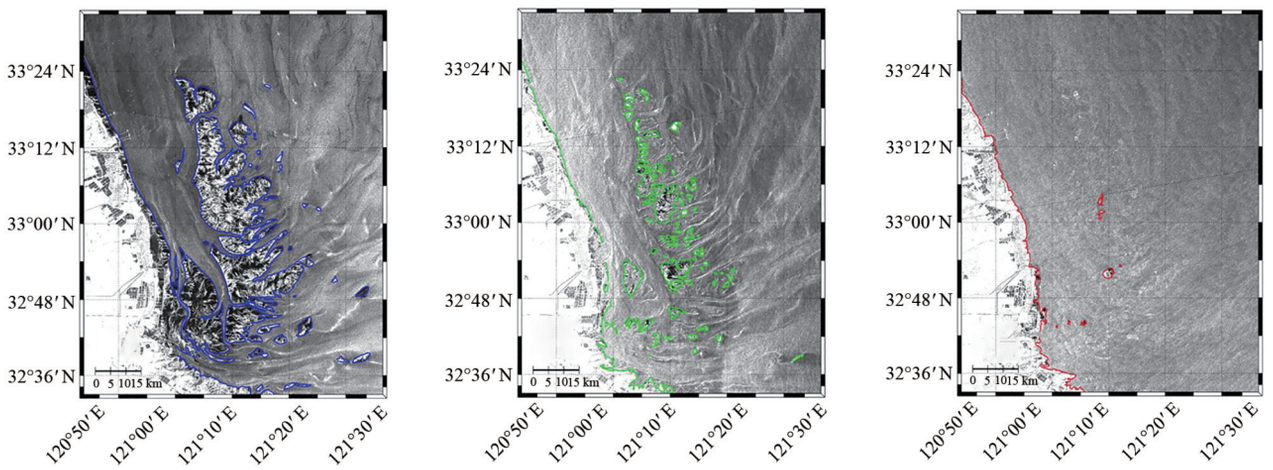

(a) low tidal level at 21:57 UTC on 2 Jun. 2015

(b) middle tidal level at 09:54 UTC on 18 Sep. 2015

(c) high tidal level at 09:54 UTC on 26 Feb. 2015. The color lines are the extracted waterlines from the SAR images

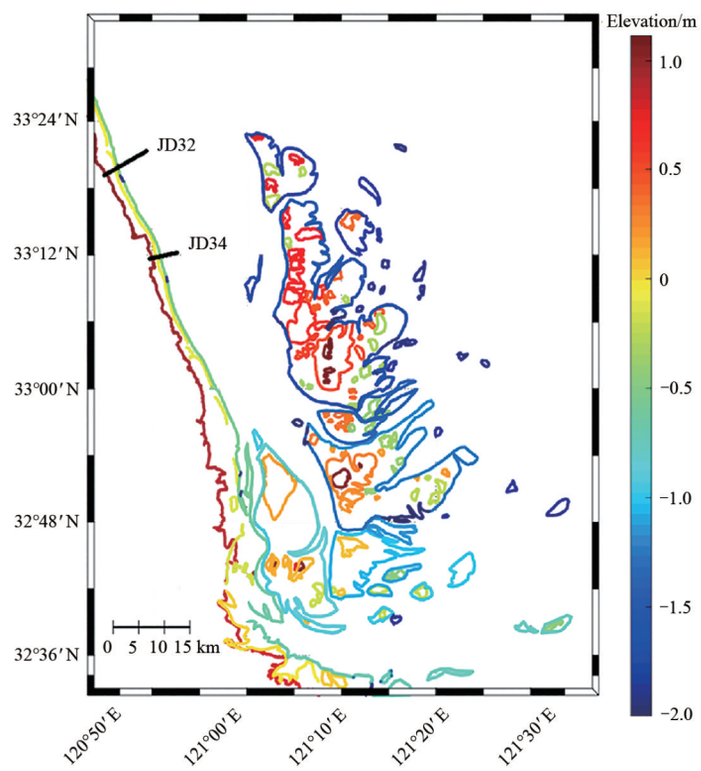

(d) SAR derived elevations using the waterline method. Comparison of SAR derived elevations (colored dots) and in-situ observations (black dots) along the two transects: JD32(e) and JD34(f)

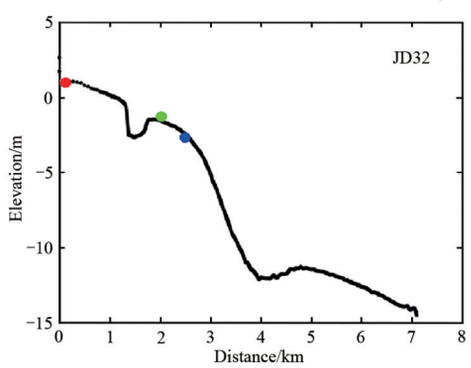

(e) JD34

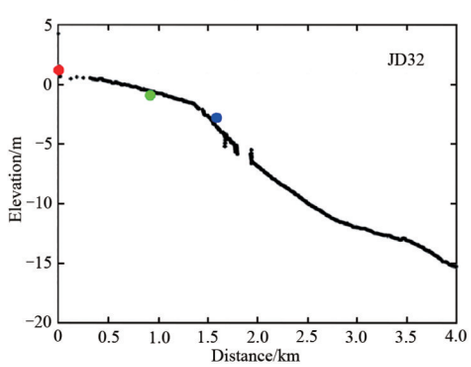

(f) JD34. The distance is measured from the left to the right for each transect

Fig.7 Three Sentinel-1A SAR images over Subei Bank acquired at different tidal levels From Zhang et al 2018

Table 2 Accuracy of water depth retrieval from high resolution satellite imagers

	Area A		Area B		Area C		Area D	
Water depth range/m	0—5.5		0—10.7		0—7.3		0—1.7	
Band type	Blue	Green	Blue	Green	Blue	Green	Blue	Green
Absolute error/m	0.36	0.39	0.86	0.81	0.49	0.50	0.06	0.07
Relative error/%	18.5	18.8	19.0	19.2	17.5	18.9	9.9	15.2

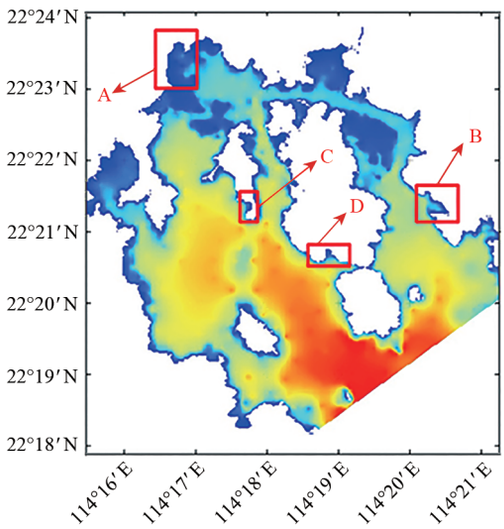

Fig.8 Test sites (A, B, C, D) in the Port Shelter of the Hong Kong coastal water

REFERENCES

Adler-Golden S M, Berk A, Bernstein L S, Richtsmeie R S, Acharya P K, Matthew M W, Aderson G P, Allred C, Jeong L, Chetwynd J H 1999. FLAASH a MODTRAN4 atmospheric correction package for hyperspectral data retrieval and simulations. Proceeding 7th Annual JPL Airborne Earth Science Workshop, 97 – 21,

Publication JPL, Pasadena, Calif., pp. 9-14.

Alpers W and Hennings I 1984. A theory of the imaging mechanism of underwater bottom topography by real and synthetic aperture radar. Journal of Geophysical Research Oceans, 89(C6): 10529-10546

Arns A, Dangendorf S, Jensen J, Talke S, Bender J and Pattiaratchi C 2017. Sea-level rise induced amplification of coastal protection design heights. Nature: Scientific Reports, 7: 40171 DOI: 10.1038/srep40171

Baselice F and Ferraioli G 2013. Unsupervised Coastal Line Extraction from SAR images. IEEE Geoscience and Remote Sensing Letters, 10(6): 1350-1354 DOI: 10.1109/LGRS.2013.2241013

Bates P D and De Roo A P J 2000. A simple raster-based model for floodplain inundation. Journal of Hydrology, 236(1-2): 54-77 DOI: 10.1016/S0022-1694(00)00278-X

Bates P D, Dawson R, Hall J, Horritt S, Nicholls J, Wicks J and Hassan M 2005. Simplified two-dimensional modelling of coastal flooding for risk assessment and planning. Coastal Engineering, 52(9): 793-810 DOI: 10.1016/j.coastaleng.2005.06.001

Bentley S J, Blum M D, Maloney J, Pond L and Paulsell R 2016. The Mississippi River source-to-sink system: Perspectives on tectonic, climatic, and anthropogenic influences, Miocene to Anthropocene. Earth-Science Reviews, 153: 139-174 DOI:10.1016/j.earscirev.2015.11.001

Berardino P, Fornaro G, Lanari R and Sansosti E 2002. A new algorithm for surface deformation monitoring based on small baseline differential SAR interferograms. IEEE Transactions on Geoscience and Remote Sensing, 40(11): 2375-2383 DOI: 10.1109/TGRS.2002.803792

Bian X, Shao Y, Tian W, Wang S, Zhang C, Wang X and Zhang Z 2017. Underwater Topography Detection in Coastal Areas Using Fully Polarimetric SAR Data. Remote Sensing, 9(6): 560 DOI: 10.3390/rs9060560

Bian X, Shao Y, Wang S, Tian W, Wang X and Zhang C 2018. Shallow water depth retrieval from multitemporal Sentinel-1 SAR data. IEEE Journal of Selected Topics in Applied Earth Observations and Remote Sensing, 99: 1-10 DOI: 10.1109/JSTARS. 2018. 2851845

Boak E H and Turner I L 2005. Shoreline definition and detection: a review. Journal of Coastal Research, 21: 688-703 DOI: 10.2112/03-0071.1

Boccia V, Renga A, Rufino G, D'Errico M, Moccia A, Aragno C and Zoffoli S 2015. Linear dispersion relation and depth sensitivity to swell parameters: Application to synthetic aperture radar imaging and bathymetry. The Scientific World Journal, 2015: 1-10 DOI: 10.1155/2015/374579

Brusch S, Held P, Lehner S, Rosenthal W and Pleskachevsky A 2011. Underwater bottom topography in coastal areas from TerraSAR-X data. International Journal of Remote Sensing, 32(16): 4527-4543 DOI: 10.1080/01431161.2010.489063

Calkoen C J, Hesselmans G H F M, Wensink G J and Vogelzang J 2001. The bathymetry assessment system: efficient depth mapping in shallow seas using radar images. International Journal of Remote Sensing, 22(15): 2973-2998 DOI: 10.1080/01431160116928

Chan C K, Yao X. 2008. Air Pollution in Megacities in China. Atmospheric Environment, 42(1): 1-42 DOI: 10.1016/j.atmosenv.2007.09.003

Chan F K S, Adekola O A, Mitchell G and McDonald A T 2013. Appraising sustainable flood risk management in the Pearl River Delta's coastal megacities: A case study of Hong Kong, China. Journal of Water and Climate Change, 4(4): 390-409 DOI: 10.2166/wcc.2013.018

Chen F, Lin H, Zhang Y and Lu Z 2012. Ground subsidence geo-hazards induced by rapid urbanization: Implications from InSAR observation and geological analysis. Natural Hazards and Earth System Sciences, 12(4): 935 – 942 DOI: 10.5194/nhess-12-935-2012

Chen J Y, Knight R, Zebker H A and Schreuder W A 2016. Confined aquifer headmeasurements and storage properties in the San Luis Valley, Colorado, from spaceborne InSAR observations. Water Resource Resarch, 52: 1 – 20 DOI:10.1002/2014WR015716

Cheng H Q, Chen J Y, Chen Z J, Ruan R L, Xu G Q, Zeng G, Zhu J R., Dai Z J, Chen X Y, Gu S H, Zhang X L, and Wang H M 2018. Mapping Sea Level Rise Behavior in an Estuarine Delta System : A Case Study along the Shanghai Coast. Engineering, 4 (1): 156 – 163 DOI:10.1016/j.eng.2018.02.002

Church J A and White N J 2006. A 20th century acceleration in global sea level rise. Geophysical Research Letters, 33: L01602 DOI: 10.1029/2005GL024826

Church J A and White N J White 2011. Sea level Rise from the Late 19th to the Early 21st Century. Surveys in Geophysics, 32(4-5): 585-602 DOI: 10.1007/s10712-011-9119-1

Covello F, Battazza F, Coletta A, Lopinto E, Fiorentino C, Pietranera L, Valentini G, and Zoffoli S 2010. COSMO-SkyMed an existing opportunity for observing the Earth. Journal of Geodynamics, 49(3-4): 171 – 180 DOI: 10.1016/j.jog.2010.01.001

Dai S B and Lu X X 2014. Sediment load change in the Yangtze River (Changjiang): A review. Geomorphology, 215: 60-73 DOI: 10.1016/j.geomorph.2013.05.027

Dai Z, Liu J T, Wei W and Chen J 2014. Detection of the Three Gorges Dam influence on the Changjiang (Yangtze River) submerged delta. Scientific Reports, 4: 6600 DOI:10.1038/srep06600

Danielson J J and Gesch D B 2011. Global Multi-Resolution Terrain Elevation Data 2010 (GMTED2010); U.S. Geological Survey Open-File Report; U.S. Geological Survey: Sioux Falls, SD, USA, 2011.

Dellepiane S, De Laurentiis R and Giordano F 2004. Coastline extraction from SAR images and a method for the evaluation of the coastline precision. Pattern Recognition Letters, 25(13): 1461 – 1470 DOI: 10.1016/j.patrec.2004.05.022

Deng X Z, Huang J K, Rozelle S, Uchida E 2008. Growth, population

and industrialization, and urban land expansion of China. Journal of Urban Economics, 63(1): 96-115 DOI: 10.1016/j. jue. 2006. 12.006

Devlin A T, Pan J, Lin H 2019a. Tidal variability in the Hong Kong region. Ocean Science, 15(4): 853-864, DOI: 10.5194/os-15-853-2019

Devlin A T, Pan J, Lin H 2019b. Extended spectral analysis of tidal variability in the North Atlantic Ocean. Journal of Geophysical Research: Oceans, 124(1): 506-526, DOI: 10.1029/2018JC014694

Ding X and Li X 2011. Monitoring of the Water-Area Variations of Lake Dongting in China with ENVISAT ASAR Images. International Journal of Applied Earth Observation and Geoinformation, 13(6): 894-901 DOI:10.1016/j.jag.2011.06.009

Ding X and Li X 2014. Shoreline movement monitoring based on SAR images in Shanghai, China. International Journal of Remote Sensing, 35(11-12): 3994-4008 DOI:10.1080/01431161.2014.916480

Domingues C M, Church J A, White N J, Glecker P J, Wijffels S E, Barker P M and Dunn J R 2008. Improved estimates of upper-ocean warming and multi-decadal sea level rise. Nature, 453: 1090-1094 DOI: 10.1038/nature07080

Duan H, Zhang H, Huang Q, Zhang Y, Hu M, Niu Y and Zhu J 2016. Characterization and environmental impact analysis of sea land reclamation activities in China. Ocean and Coastal Management, 130: 128-137 DOI:10.1016/j.ocecoaman.2016.06.006

Falabella F, Pepe A, Zhao Q, Guanyu M., Serio C, Lanari R 2018. A hybrid multi-scale InSAR approach to study the 2014-2018

Surface Deformation of the Shanghai Coastal Region through Sequences of Time-Gapped Cosmo-SkyMed SAR acquisitions. ESA-MOST Dragon IV Mid-term Symposium, Xi'an, China, June 2018.

Familkhalili R and Talke S A 2016. The Effect of Channel Deepening on Storm Surge: Case Study of Wilmington, NC. Geophysical Research Letters, 43(17): 9138-9147 DOI:10.1002/2016GL069494

Fan K, Huang W, Lin H, Pan J, Fu B and Gu Y 2011. Shallow water depth retrieval from space-borne SAR imagery. Journal of oceanography, 67(4): 405-413

Ferretti A, Prati C and Rocca F 2001. Permanent scatterers in SAR interferometry. IEEE Transactions on Geoscience and Remote Sensing, 39(1): 8-20 DOI: 10.1109/36.898661

Ferretti A, Fumagalli A, Novali F, Prati C, Rocca V and Rucci A 2011. A New Algorithm for Processing Interferometric Data-Stacks: SqueeSAR. IEEE Transactions on Geoscience and Remote Sensing, 49(9): 3460-3470 DOI: 10.1109/TGRS.2011.2124465

Feng X, Tsimplis M N and Woodworth P L 2015. Nodal variations and long-term changes in the main tides on the coasts of China. Journal of Geophysical Research: Oceans, 120(2): 1215-1232 DOI: 10.1002/2014JC010312

Franceschetti G and Lanari R 1999. Synthetic Aperture Radar Processing; CRC Press: Boca Raton, FL, USA.

Freeman A 1992. SAR Calibration: An overview. IEEE Transactions on Geoscience and Remote Sensing, 30(6):1107-1121 DOI: 10.1109/36.193786

Fugura A A, Billa L and Pradhan B 2011. Semi-automated procedures for shoreline extraction using single RADARSAT-1 SAR image. Estuarine, Coastal and Shelf Science, 95(4): 395-400 DOI: 10.1016/j.ecss.2011.10.009

Gesch D B 1999. Chapter 31

– The effects of DEM generalization methods on derived hydrologic features, Lowellin, Kim, and Jaton, Annick, eds., Spatial Accuracy Assessment—Land Information Uncertainty in Natural Resources: Chelsea, Mich., Ann Arbor Press, 255-262.

Geyman E C, and Maloof A C 2019. A simple method forextracting water depth from multi-spectral satellite imagery in regions of variable bottom type. Earth and Space Science, 6: 527-537 DOI: 10.1029/2018EA000539.

Gong P, Liang S, Carlton E J, Jiang Q, Wu J, Wang L, Remais, J V 2012. Urbanization and Health in China. Lancet, 379(9818): 843-852 DOI: 10.1016/S0140-6736(11)61878-3

He L, Li G S, Li K and Shu Y Q 2014. Estimation of regional sea level change in the Pearl River Delta from tide gauge and satellite altimetry data, Estuarine, Coastal and Shelf Science, 141: 69-77.

Higgins S A 2016. Review: Advances in delta-subsidence research using satellite methods. Hydrogeology Journal, 24(3): 587-600 DOI: 10.1007/s10040-015-1330-6

Hooper A, Zebker H, Segall P and Kampes B M 2004. A new method for measuring deformation on volcanoes and other natural terrains using InSAR persistent scatterers. Geophysical Research Letters, 31(23): L23611 DOI: 10.1029/2004GL021737

Huang H, Chen X, Zhu Z, Xie Y, Liu L, Wang X, Wang X and Liu K 2018. The changing pattern of urban flooding in Guangzhou, China. Science of Total Environment, 622-623: 394-404. DOI: 10.1016/j.scitotenv.2017.11.358

Huang W and Fu B 2004. A spaceborne SAR technique for shallow water bathymetry surveys. Journal of Coastal Research, 43: 223-228.

Ingbritsen S E, Ikehara M E, Galloway D L and Jones D R 2000. Delta Subsidence in California: The sinking heart of the State Fact Sheet 005-00. Water Resour. 75: E66-72 DOI: 10.3133/fs00500

Jan S, Chern C S, Wang J and Chao S Y 2007. Generation of diurnal K1 internal tide in the Luzon Strait and its influence on surface tide in the South China Sea. Journal of Geophysical Research: Oceans, 112(C6): C06019 DOI: 10.1029/2006JC004003

Jan S, Lien R C and Ting C H 2008. Numerical study of baroclinic tides in Luzon Strait. Journal of Oceanography, 64(5): 789-802 DOI: 10.1007/s10872-008-0066-5

Jarvis A, Reuter H I, Nelson A and Guevara E 2008. Hole-filled SRTM for the globe Version 4. available from the CGIAR-CSI SRTM 90m Database <http://srtm. csi.cgiar. org>.

Jay D A 2009. Evolution of tidal amplitudes in the eastern Pacific Ocean. Geophysical Research Letters, 36: L04603 DOI: 10.1029/2008GL036185

Jiang C, Li J and de Swart H E 2012. Effects of navigational works on morphological changes in the bar area of the Yangtze Estuary. Geomorphology, 139-140: 205-219 DOI: 10.1016/j. geomorph.2011.10.020

Jin M, Zhang J and Yuan Y 1998. Analysis of bathymetric features using SAR image: An example from the southern North Sea. Chinese Journal of Oceanology and Limnology, 16(2): 128-136.

Kang Y, Ding X, Xu F, Zhang C and Ge X 2017. Topographic mapping on large-scale tidal flats with an iterative approach on the waterline method. Estuarine, Coastal and Shelf Science, 190: 11-22.

Köhl A, Stammer D and Cornuelle B 2007. Interannual to decadal changes in the ECCO global synthesis. Journal of Physical Oceanography, 37(2): 313-337 DOI: 10.1175/JPO3014.1

Krieger G, Moreira A, Fiedler H, Hajnsek I, Werner M, Younis M and Zink M 2007. TanDEM-X: A satellite formation for high-resolution SAR interferometry. IEEE Transactions on Geoscience and Remote Sensing, 45(11): 3317-3341 DOI: 10.1109/TGRS. 2007. 900693

Kuang C, Chen W, Gu J, Su T-C, Song H, Ma Y and Dong Z 2017. River discharge contribution to sea-level rise in the Yangtze River Estuary, China. Continental Shelf Research, 134: 63-75 DOI: 10.1016/j.csr.2017.01.004

Lanari R., Mora O., Manunta M, Mallorqui J J, Berardino P, Sansosti E. 2004. A Small Baseline Approach for Investigating Deformation on Full resolution Differential SAR Interferograms, IEEE Transactions Geoscience and Remote Sensing, 42(7): 1377-1386 DOI: 10.1109/TGRS.2004.828196

Lee 1981. Speckle analysis and smoothing of Synthetic Aperture Radar images. Computer Graphics and Image Processing, 17(1): 24-32 DOI: 10.1016/S0146-664X(81)80005-6

Lee J-S and Jurkevich I 1990. Coastline Detection and Tracing in SAR Images. IEEE Transactions on Geoscience and Remote Sensing, 28 (4): 662-668 DOI:10.1109/TGRS.1990.572976.

Lee Z, Carder K L, Mobley C D, Steward R G, and Patch J S 1998. Hyperspectral remote sensing for shallow waters. I. a semianalytical model. Applied Optics. 37(27): 6329-6338.

Li, KW, and Mok, H Y 2012. Long term trends of the regional sea level changes in Hong Kong and the adjacent waters. In Asian And Pacific Coasts 2011 (pp. 349-359. DOI: 10.1142/9789814366489_0040

Lyzenga D R 1978. Passive remote sensing techniques for mapping water depth and bottom features. Applied Optics, 17(3): 379-383.

De Loor G P 1981. The observation of tidal patterns, currents, and bathymetry with SLAR imagery of the sea. IEEE Journal of Oceanic Engineering, 6(4):124-129.

De Loor G P and Hulten H W B V 1978. Microwave measurements over the North Sea Boundary-Layer. Meteorology, 13(1-4): 119-131.

Luan H L, Ding P X, Wang Z B, Ge J Z and Yang S L 2016. Decadal morphological evolution of the Yangtze Estuary in response to river input changes and estuarine engineering projects. Geomorphology, 265: 12-23 DOI:10.1016/j.geomorph.2016.04.022

Mason D C, Scott T R, Dance S L 2010. Remote sensing of intertidal morphological change in Morecambe Bay, U.K., between 1991 and 2007. Estuarine, Coastal and Shelf Science, 87(3): 487-496 DOI: 10.1016/j.ecss.2010.01.015

Massonnet D and Feigl K L 1998. Radar interferometry and its application to changes in the Earth's surface. Reviews of Geophysics, 36 (4): 441–500 DOI: 10.1029/97RG03139

Mei X, Dai Z, Wei W, Li W, Wang J and Sheng H 2018. Secular bathymetric variations of the North Channel in the Changjiang (Yangtze) Estuary, China, 1880-2013: Causes and effects. Geomorphology, 303: 30-40 DOI:10.1016/j.geomorph.2017.11.014

Merrifield M A, Merrifield S T.and Mitchum G T 2009. An anomalous recent acceleration of global sea level rise. Journal of Climate, 22 (21): 5772-5781 DOI: 10.1175/2009JCLI2985.1

Merrifield M A 2011. A shift in Western tropical Pacific sea level trends during the 1990s. Journal of Climate, 24: 4126-4138 DOI: 10.1175/2011JCLI3932.1

Mishra M K, Ganguly D and Chauhan P 2014. Estimation of coastal bathymetry using RISAT-1 C-band microwave SAR data. IEEE Geoscience and Remote Sensing Letters, 11(3): 671-675 DOI: 10.1109/LGRS.2013.2274475

Moftakhari H R, AghaKouchak A, Sanders B F, Feldman D L, Sweet W, Matthew R A and Luke A 2015. Increased nuisance flooding along the coasts of the United States due to sea level rise: Past and future. Geophysical Research Letters, 42(22): 9846-9852 DOI: 10.1002/2015GL066072

Moftakhari H R, AghaKouchak A, Sanders B F and Matthew R A 2017. Cumulative hazard: The case of nuisance flooding. Earth's Future, 5(2):14-223 DOI: 10.1002/2016EF000494

Mukherjee S, Joshi P, Mukherjee S, Ghosh A, Garg R and Mukhopadhyay A 2013. Evaluation of vertical accuracy of open source Digital Elevation Model (DEM). International Journal of Applied Earth Observation and Geoinformation, 21: 205–217 DOI: 10.1016/j.jag.2012.09.004

Mora O, Mallorqui J J and Broquetas A 2003. Linear and nonlinear terrain deformation maps from a reduced set of interferometric SAR images. IEEE Transactions on Geoscience and Remote Sensing, 41(10): 2243-2253 DOI: 10.1109/TGRS.2003.814657

Nerem R S, Chambers D P, C and MitchumChoe, G T 2010. Estimating mean sea level change from the TOPEX and Jason altimeter missions. Marine Geodesy, 33(S1): 435-446 DOI: 10.1080/01490419.2010.491031

Nicholls R. J and Cazenave A 2010. Sea Level Rise and Its Impact on Coastal Zones. Science, 80(328): 1517-1520 DOI: 10.1126/science.1185782

Pan C, Wang X, Liu L, Huang H and Wang D 2017. Improvement to the huff curve for design storms and urban flooding simulations in Guangzhou, China. Water (Switzerland), 9: 1-18. DOI: 10.3390/w9060411

Pan L and Ge J 2011. Analysis of the influence of Deep Waterway Project on morphological evolution in the north passage of the Changjiang Estuary, China. Proceedings of 2011

International Conference on Remote Sensing, Environment Transportation Engineering, Nanjing, June, 2011

Pardo-Pascual J E, Sánchez-García E, Almonacid-Caballer J, Palomar-Vázquez J M, Priego de los Santos E, Fernández-Sarría A and Balaguer-Beser Á 2018. Assessing the Accuracy of Automatically Extracted Shorelines on Microtidal Beaches from Landsat 7, Landsat 8 and Sentinel-2 Imagery. Remote Sensing, 10: 326. DOI: 10.3390/rs10020326

Pepe A and Lanari R 2006. On the extension of the minimum cost flow algorithm for phase unwrapping of multi-temporal differential SAR interferograms. IEEE Transactions on Geoscience and Remote Sensing, 44(9): 2374-2383 DOI: 10.1109/TGRS. 2006. 873207

Pepe A, Bonano M, Zhao Q, Yang T and Wang H 2016. The Joint Use of Multiple Satellite SAR Data and Geotechnical Models for the Study of the Shanghai Ocean-Reclaimed Lands. Remote Sensing, 8: 911 DOI:10.20944/preprints201608.0083.v1

Pepe A and Calò F 2017. A Review of Interferometric Synthetic Aperture RADAR (InSAR) Multi-Track Approaches for the Retrieval of Earth's Surface Displacements. Applied Sciences, 2017(12): 1264; DOI: 10.3390/app7121264.

Polcyn F C, Brown W L, and Sattinger I J 1970. The Measurement of Water Depth by Remote Sensing Techniques, Report 8973-26-F, Willow Run Laboratories, The University of Michigan, ArborAnn.

Ray R D 2006. Secular changes of the M2 tide in the Gulf of Maine. Continental Shelf Research, 26(3): 422-427 DOI: 10.1016/j.csr.2005.12.005

Ray R D 2009. Secular changes in the solar semidiurnal tide of the Western North Atlantic Ocean. Geophysical Research Letters 36: L19601 DOI: 10.1029/2009GL040217

Ray R D and Foster G 2016. Future nuisance flooding at Boston caused by astronomical tides alone. Earth's Future, 4(12): 578-587 DOI: 10.1002/2016EF000423

Ren M E 1993. Relative Sea level changes in China over the last 80 years, Journal of Coastal Research, 9 (1): 229-241.

Renga A, Rufino G, D'Errico M, Moccia A, Boccia V, M DGrazianoet al. 2014. SAR bathymetry in the Tyrrhenian Sea by COSMO-SkyMed data: A novel approach. IEEE Journal of Selected Topics in Applied Earth Observations and Remote Sensing, 7(7): 2834-2847 DOI: 10.1109/JSTARS.2014.2327150

Ryu J H, Won J S, Min K D 2002. Waterline extraction from Landsat TM data in a tidal flat: a case study in Gomso Bay, Korea. Remote sensing of Environment, 83(3): 442-456 DOI: 10.1016/S0034-4257(02)00059-7

Simms A, Reynolds L C, Bentz M, Roman A, Rockwell T and Peters R 2016. Tectonic Subsidence of California Estuaries Increases Forecasts of Relative Sea-Level Rise. Estuaries and Coasts, 39: 1571-1581 DOI:10.1007/s12237-016-0105-1

Slangen A B, Church J A, Agosta C, Fettweis X, Marzeion B and Richter K 2016. Anthropogenic forcing dominates global mean sea-level rise since 1970. Nature Climate Change, 6(7): 701-705, DOI: 10.1038/nclimate2991

Stewart C, Renga A, Gaffney V and Schiavon G 2016. Sentinel-1 bathymetry for North Sea palaeo landscape analysis. International Journal of Remote Sensing, 37(3): 471-491 DOI: 10.1080/01431161.2015.1129563